Reducing HVDC Network Oscillations Considering Wind Intermittency Through Optimized Grid Expansion Decision

Atousa Elahidoost
Department of Electric Power Engineering
Norwegian University of Science and Technology (NTNU)
Trondheim, Norway
atousa.elahidoost@ntnu.no

Luca Furieri
Automatic Control Laboratory
Swiss Federal Institute of Technology (ETH)
Zurich, Switzerland
furieril@control.ee.ethz.ch

Elisabetta Tedeschi
Department of Electric Power Engineering
Norwegian University of Science and Technology (NTNU)
Trondheim, Norway
elisabetta.tedeschi@ntnu.no

Maryam Kamgarpour
Automatic Control Laboratory
Swiss Federal Institute of Technology (ETH)
Zurich, Switzerland
mkamgar@control.ee.ethz.ch

***Abstract*—This paper considers the evolution of independent offshore HVDC links into a multi-terminal network. It proposes a control strategy to maximize the DC voltage stability under the worst-case perturbation scenario and considers the intermittent nature of the power injection from connected wind farms. A decentralized linear feedback controller achieving the minimization of the DC voltage oscillations, while ensuring control input constraints (i.e. reference currents) compliance, is proposed. The motivation of this framework is to include the DC voltage stability maximization under the worst-case perturbation as an additional decision criterion in a multi-objective optimization for HVDC network expansion decision. The other criteria can include for instance, length or cost of a line or the power losses along the line. To evaluate the applicability of the proposed method, placement of a new HVDC link between two independent VSC-based point-to-point HVDC grids located in the North Sea is assessed, using real wind data for a 4-terminal test grid.**

Keywords—DC voltage stability index, offshore HVDC grid, optimal linear feedback controller, voltage stability, wind intermittency

I. INTRODUCTION

In recent years there is a global tendency towards the increasing implementation and improvement of renewable energy conversion technologies, especially solar and wind, in response to the realization of smart grid policies. The motivation for integrating renewables into the global energy network is not only to meet the increasing energy demand, but also to improve the energy availability, reliability, security and quality, as well as to compensate the adverse impact of fossil fuels on global warming.

Wind energy is one of the most promising renewable energy resources. In Europe, during 2017, 15.6 GW of new wind energy capacity was connected to the power grid, of which 12.5 GW were installed onshore and 3.2 GW offshore [1]. Offshore wind resources are expected to account for more than one fifth of the total wind capacity in Europe by 2030 [2] and the need to transmit such huge amounts of power to shore will require the deployment of offshore HVDC networks.

The focus of this paper is on stability and control of the offshore HVDC-based wind farms located in the North Sea. The goal is to emphasize the significance of system dynamics' considerations, together with the role that wind stochasticity and DC cable losses can play in any grid expansion decision. The majority of the existing or planned HVDC links are represented by point-to-point connections. The gradual interconnection of the existing point-to-point and newly designed HVDC grids into multi-terminal and meshed networks in the North Sea is a prerequisite for the implementation of an 100% renewable European smart grid [3]. In such highly interconnected HVDC networks, keeping the DC voltage constant in steady state condition and within a predefined range during dynamics and transients is of paramount importance, and it is an indicator of power balance and stability in the grid [4]. Additionally, DC voltage resonances due to the non-passive behavior of the Voltage Source Converters (VSCs) are considered as a source of instability in HVDC networks and should be avoided [5].

Due to the expected growth of HVDC networks, the most recent literature in transmission expansion planning (TEP) investigates the hybrid AC/DC grid expansion challenges and opportunities [6-10]. The main objective in TEP problems is generally to minimize costs and power losses. Control and stability criteria are seldom considered as expansion decision variables in hybrid AC/DC multi-terminal networks dominated by intermittent energy resources [11]. For instance, [12] is one of the few references that has considered small signal stability enhancement as a means to improve hybrid AC/DC smart grid reliability and security in expansion planning. However, the focus is only on stability improvement on the AC side, and the DC voltage resonance risks have not been taken into account. Additionally, renewable energy intermittency is also a decisive criterion in grid expansion problems in the case of high penetration of solar or wind. Reference [13] integrates the wind intermittency effect into a robust day-ahead scheduling problem with multi-terminal VSC-HVDC network through a mixed integer linear programming (MILP) optimization approach. The proposed MILP method can efficiently compute a linearized AC optimal power flow (ACOPF) in large-scale systems.

The aim of this paper is trifold. First, to account for the wind intermittency in optimized offshore HVDC placement based on real wind data. The goal is to show that the stability considerations performed with respect to the nominal operating point are not sufficient in view of the grid expansion decision and a more comprehensive analysis accounting for wind variability is necessary. Second, we design a decentralized linear feedback controller, which is

optimal for the worst-case initial state perturbation. Additionally, our technique allows complying with input constraints for a realistic range of variability of the initial state perturbations. Third, the effect of the DC line losses as further expansion criterion is also taken into account.

II. Theory and Methodology

A. Wind Energy Data Analysis

In this section, the wind variability effect on power extraction of HVDC offshore wind farms based on real wind datasets is analyzed. For this purpose, wind data time series are extracted for two locations in the North Sea. They are based on the Reanalysis dataset providing the average wind speed with a spatial resolution of 2.5 degrees and a temporal resolution of 6 hours in the years 2001-2005 [14]. The selected offshore sites are Johan-Sverdrup, Norway, and BorWin1, Germany. Linear interpolation has been applied in order to obtain hourly time series at the selected points. Wind speed time series correspond to the height of 45 m above the sea surface and since wind turbines' hub height are typically higher (around 100 m); adjustment factors based on [15] are used in wind power time series calculation.

Fig. 1a-b show the histograms of hourly wind speed at the two locations at the height of 45 m for the 5-year period. The average wind speed at Johan-Sverdrup is about 8.67 m/s and at BorWin1 is approximately 8.26 m/s, and min/max values are 0.63/29.47 m/s and 0.78/28.27 m/s, respectively. It is apparent from the histogram that wind data can be well fit into the Weibull probability distribution function. The normalized mean wind power curves (Fig. 1c-d) for the two locations are indeed average power curves for several wind turbines in the regions obtained by fitting power-speed dataset into a polynomial curve.

Wind power time series are computed as a function of normalized mean wind power curves with the product of wind speed time series and adjustment factors as inputs:

$$P = f\,(aV), \tag{1}$$

where f is the normalized mean wind power curve, a is the adjustment factor, and V is the wind speed. The adjustment factors are used to compensate for discrepancies between the actual and computed wind energy and are extracted according to [14]. Histograms of the normalized wind power for the two offshore sites are depicted in Fig. 1e-f. It is worth noting that at both locations, the probability that wind farms produce 10% of the nominal power is the highest, and the second highest corresponds to 90% of the nominal power production.

It is assumed there is a demand to connect the BorWin1 wind farm to another wind farm to be constructed at Johan-Sverdrup site via an offshore HVDC cable. Then, in order to quantify the total wind power production in the resultant HVDC network, the simultaneous occurrence of the normalized power in 4 ranges (0-0.25 pu, 0.25-0.5 pu, 0.5-0.75 pu, and 0.75-1 pu) at the two farms is evaluated. The results are presented in Table I. The intersection of the normalized power range of 0-0.25 pu at both places can be interpreted as follows. There is 22% probability that the two

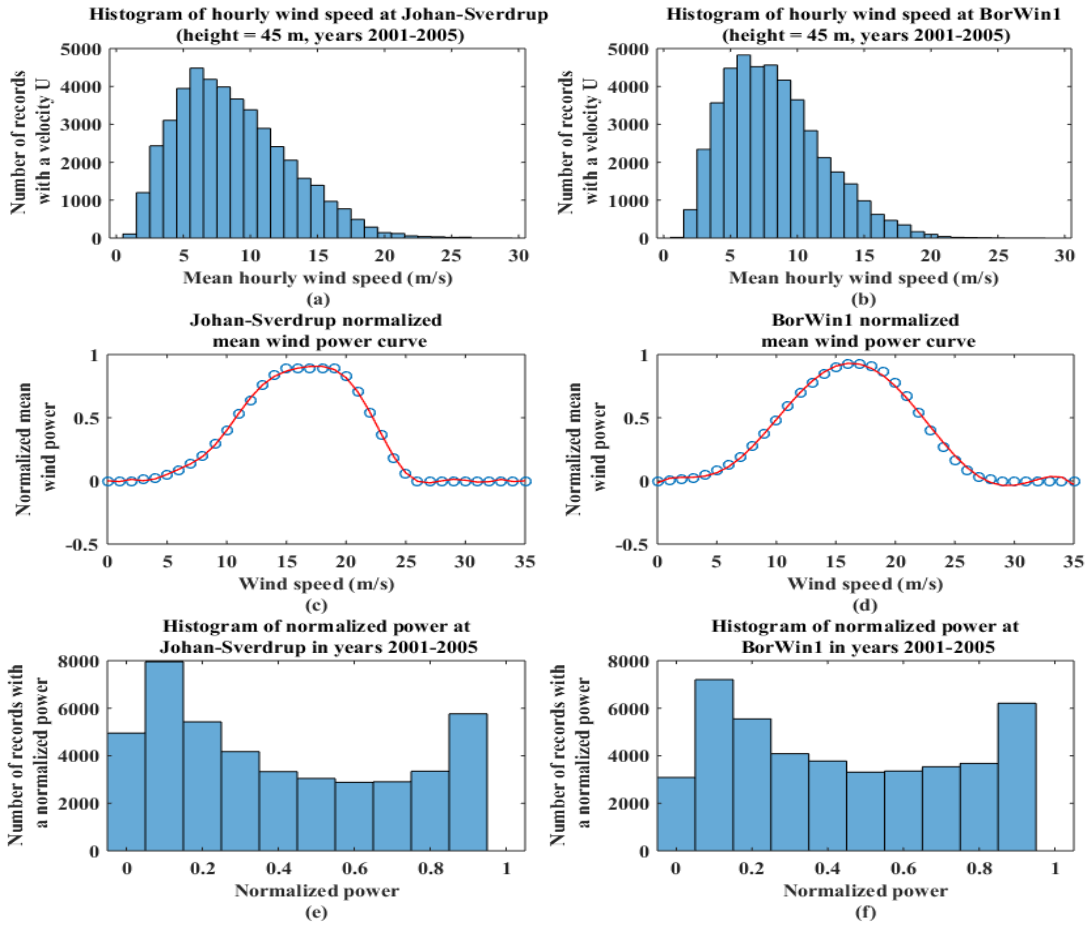

Fig. 1: Johan-Sverdrup and BorWin1 (a-b) hourly wind speed histograms, (c-d) normalized mean wind power curves and (e-f) normalized power histograms.

Table I: Probability of simultaneous occurrence of normalized power at Johan-Sverdrup and BorWin1 locations (Base power: 1200 MVA).

Normalized power ranges in per unit		BorWin1			
		0 - 0.25	0.25 - 0.5	0.5 - 0.75	0.75 - 1
Johan-Sverdrup	0 - 0.25	0.22	0.09	0.06	0.04
	0.25 - 0.5	0.07	0.05	0.04	0.04
	0.5 - 0.75	0.04	0.04	0.04	0.05
	0.75 - 1	0.03	0.04	0.05	0.09

wind farms generate power in the range of 0-0.25 pu at the same time.

B. HVDC-VSC Based Grid Configuration and Modelling

A four-terminal HVDC grid based on the configuration and parameters reported in [16] is considered as the test system, whose structure is given in Fig. 2. It is assumed that cable 1-2 is representative of HVDC link from Johan-Sverdrup to the onshore grid in Norway with 200 kilometers length whereas cable 3-4 is a point-to-point HVDC link between BorWin1 and Germany (200 km). It is further considered that there is a plan for interconnection of the two networks. The goal is to improve the grid availability. Given the weather-dependent wind farms' productivities, the challenge is to select the line, which ensures the best grid operation subject to dynamics and transients, while minimizing power losses. It should also be noted that in selecting the HVDC link, environmental and regulatory constraints, such as water depth restrictions or Exclusive Economic Zones (EEZ) are not taken into account.

For a preliminary assessment, the four converters in offshore and onshore substations are considered to be three-phase 2-Level Voltage Source Converters (2-L VSC), which are modeled in the synchronous *dq0* reference frame in per unit. A simplified architecture of the 2-L VSC and the corresponding control are shown in Fig. 3 [17]. In order to apply the selected optimization methodology, the entire HVDC grid, consisting of converters with inner current controllers and cables, needs to be linearized around an equilibrium point and represented through the state-space equations (2) and (3).

$$\Delta\dot{x}(t) = A\Delta x(t) + B\Delta u(t), \tag{2}$$

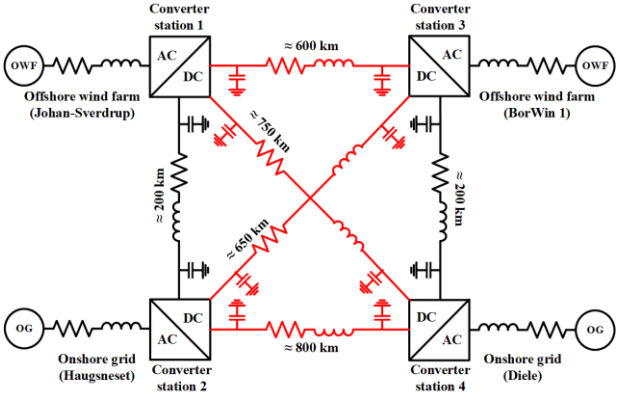

Fig. 2: 4-terminal HVDC test grid: existing links (black lines) and possible expansions considered (red lines).

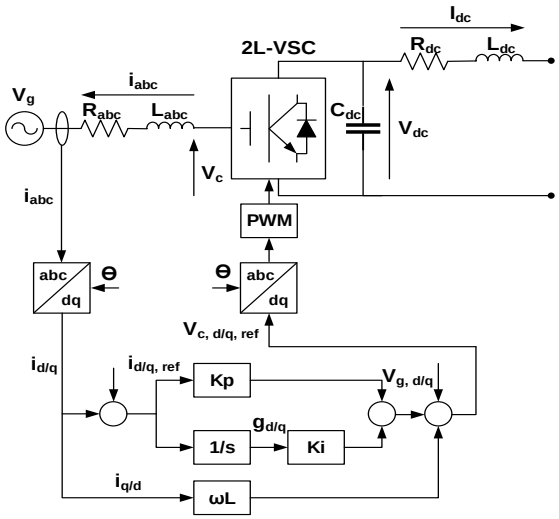

Fig. 3: Simplified model of the considered 2L-VSC [17].

$$\Delta z(t) = C\Delta x(t). \tag{3}$$

The state vector, $\Delta x(t)$, containing 23 elements, is composed of converters' *dq*-axis AC current components' variation ($\Delta i_{d/q,n}$, *n=1-4*), inner current controller *dq*-axis AC current integral components' variation ($\Delta g_{d/q,n}$, *n=1-4*), and DC voltage variations ($\Delta v_{dc,n}$, *n=1-4*) as well as DC cables' current variation ($\Delta i_{dc,ab}$, *ab=12, 34, …*). The state vector corresponding to the configuration with link 1-3 is given as an example,

$$\begin{aligned}\Delta x_{1-3}(t) = [&\Delta i_{d,1}, \Delta i_{q,1}, \Delta v_{dc,1}, \Delta g_{d,1}, \Delta g_{q,1}, \Delta i_{d,2}, \Delta i_{q,2}, \Delta v_{dc,2}, \ldots \\ &\Delta g_{d,2}, \Delta g_{q,2}, \Delta i_{dc,12}, \Delta i_{d,3}, \Delta i_{q,3}, \Delta v_{dc,3}, \Delta g_{d,3}, \Delta g_{q,3}, \ldots \\ &\Delta i_{d,4}, \Delta i_{q,4}, \Delta v_{dc,4}, \Delta g_{d,4}, \Delta g_{q,4}, \Delta i_{dc,34}, \Delta i_{dc,13}],\end{aligned} \tag{4}$$

where we dropped the explicit dependence on time of the components of $\Delta x_{1\text{-}3}(t)$ to simplify the notation.

The control input vector, $\Delta u(t)$, is composed of *dq*-axis components of the converters' reference AC current variation, i.e.

$$\begin{aligned}\Delta u(t) = [&\Delta i_{d,ref,1}, \Delta i_{q,ref,1}, \Delta i_{d,ref,2}, \Delta i_{q,ref,2}, \\ &\Delta i_{d,ref,3}, \Delta i_{q,ref,3}, \Delta i_{d,ref.4}, \Delta i_{q,ref,4}].\end{aligned} \tag{5}$$

The output vector, $\Delta z(t)$, which is a subset of the desired state variables, consists of converters' DC voltage variations where the goal is to minimize them.

$$\Delta z(t) = [\Delta v_{dc1}, \Delta v_{dc2}, \Delta v_{dc3}, \Delta v_{dc4}]. \tag{6}$$

Given the linearized model around a specific equilibrium point, we aim to solve an optimization problem to identify the best performance in the worst-case perturbation scenario. The cost function of this problem represents a "DC voltage stabilization index" and can be expressed as the integral of $z(t)$ squared over time until steady-state. The problem is subject to input constraints, which have to be satisfied for any realization of the initial state perturbations. We model input constraints as coupled ellipsoidal constraints on $\Delta i_{d,\,ref,\,n}$ and $\Delta i_{q,\,ref,\,n}$ for every converter station. From a physical point of view, this reflects the way the total current limitation of 2-L VSC couples the admitted AC current variations on the *d* and *q* axes of each converter. At the same time, the

ellipsoidal constraint takes into account that the current capability of each converter does not affect the current capabilities of converters at the other terminals. Given the diverse nature of the scalar state variables in (4), we also model the initial state perturbations as separate ellipsoidal sets or intervals for different sets of state variables. For instance, we assume that $\Delta i_{d,n}$ and $\Delta i_{q,n}$ belong to a different 2-dimensional ellipsoid for each n, while we assume that $\Delta v_{dc,n}$ belongs to an interval for each n. We consider a total of 15 separate ellipsoidal sets of perturbations for different initial state variables, which yields more realistic results than [17] and requires manipulation of the optimization problems involved.

C. Optimization Problem Derivation

The optimization methodology applied in this paper is based on Semi Definite Programming (SDP) and is an extension of the approach introduced in [18, 19]. The motivation to select the technique in [18] is twofold. First, it offers the possibility of tackling a bi-level optimization problem in a tractable way. In particular, the procedure identifies the worst-case initial state perturbation and jointly computes a linear feedback controller, which is optimal against this specific perturbation. Second, the procedure allows complying with the physical constraints of the inputs (4) considering realistic initial state perturbation sets. The original scope in [18, 19] is on AC grid reinforcement by placement of the best HVDC link. However, the focus in this paper is to identify the best location of an added HVDC link in order to maximize the DC voltage stability.

An extension of the optimization method [18, 19] aimed at decoupling the constraints on the control input signals of every converter station has been proposed in [17]. Here, we further extend the technique of [17] in order to address more realistic perturbations on the initial state variables as per Section II-B.

a) Problem Formulation: We consider a continuous-time linear system in the form

$$\begin{aligned} \dot{x}(t) &= A\,x(t) + B\,u(t) \\ \mathrm{z}(t) &= C\,x(t) \\ u(t) &= Kx(t) \end{aligned} \quad , \tag{7}$$

where $x(t) \in \mathbb{R}^n$, $u(t) \in \mathbb{R}^m$, $z(t) \in \mathbb{R}^p$, and K is the decentralized optimal linear controller ensuring the best performance under the worst-case perturbation scenario. In accordance with the discussion in Section II-B, the optimization problem for a specific network configuration and a specific operating equilibrium point can be formulated as follows.

$$\begin{aligned} &J = \min_{K} \max_{x(0)\in\chi_0} \int_0^\infty z(t)^T\, z(t)\, dt \\ &\text{s.t. (7), } (A+BK) \text{ is asympt. stable, } K \text{ is decentralized,} \\ &\forall x(0) \in \chi_0,\ \forall t : u(t) \in U, \end{aligned} \tag{8}$$

where the sets χ_0 and U are defined as follows:

$$\begin{aligned} \chi_0 &= \left\{ x = \left[x_1^T \ \dots \ x_r^T \right]^T,\ x_i \in \mathbb{R}^{n_i} \,\middle|\, \forall i \in \mathbb{Z}_{[1,r]}\ x_i^T E_x^i x_i \le 1 \right\}, \\ U &= \left\{ u = \left[u_1^T \ \dots \ u_q^T \right]^T,\ u_j \in \mathbb{R}^{m_j} \,\middle|\, \forall j \in \mathbb{Z}_{[1,q]}\ u_j^T E_u^j u_j \le 1 \right\}, \end{aligned} \tag{9}$$

Clearly $\sum_{i=1}^{r} n_i = n$ and $\sum_{j=1}^{q} m_i = m$. The matrices $E_x^i > 0$ and $E_u^j > 0$ in (9) are symmetric positive definite matrices, which define the range of admissible perturbations on the initial states and the constraints on the input variables.

We require that controllers at each converter station only know local state information. For example, the controller at converter station 1, in the case that the link 1-3 is added, only knows $\Delta i_{d,1}$, $\Delta i_{q,1}$, $\Delta v_{dc,1}$, $\Delta g_{d,1}$, $\Delta g_{q,1}$, $\Delta i_{dc,12}$ and $\Delta i_{dc,13}$. To ensure this, only those specific entries of K corresponding to available state information are allowed to be assigned a value, while those corresponding to unavailable state information are constrained to be null.

In the case in which $n_i = m_j = 1, \forall i, j$, the problem is equivalent to the one studied in [18, 19]. For $m_j \ge 1$, the problem is equivalent to the one studied in [17]. Here, we address the general case where n_i and m_j are both integer values larger than 1.

b) Formulation of the Worst-Case Performance J: It is known based on the Lyapunov stability theory that if $(A+BK)$ is asymptotically stable, then

$$\int_0^\infty x(t)^T C^T C\, x(t)\, dt = x(0)^T P\, x(0), \tag{10}$$

where $P > 0$ is the unique symmetric positive definite solution to $P(A+BK) + (A+BK)^T P + C^T C = 0$. Now, we focus on the inner maximization of (8), which is equivalent to maximization of the term $x(0)^T P\, x(0)$ over the set χ_0. Since $E_x^i > 0$ for every $i \in \mathbb{Z}_{[1,r]}$, we can compute

$$E_x^i = \hat{E}_x^i \hat{E}_x^{iT}, \quad \hat{E}_x^i = V_x^i D_x^{i\frac{1}{2}},$$

where the columns of V_x^i contain the eigenvectors of E_x^i and $D_x^{i\frac{1}{2}}$ contains the square root of the eigenvalues of E_x^i on its diagonal. We define $\tilde{x}_i$ such that $x_i = (\hat{E}_x^i)^{-T} \tilde{x}_i$. To obtain a tractable formulation of (8)-(9), we impose the following restriction on matrix P.

Restriction: Matrix P is required to be block-diagonal and its i-th block P_i must have dimensions $n_i \times n_i$.

Given the restriction above, we have

$$\begin{aligned} \max_{x_0 \in \chi_0} x(0)^T P\, x(0) &= \sum_{i=1}^{r} \max_{\|\tilde{x}_i\|_2 \le 1,\ \forall i \in \mathbb{Z}_{[1,r]}} \tilde{x}_i^T (\hat{E}_x^i)^{-1} P_i (\hat{E}_x^i)^{-T} \tilde{x}_i \\ &= \sum_{i=1}^{r} \lambda_{\max}\left((\hat{E}_x^i)^{-1} P_i (\hat{E}_x^i)^{-T}\right). \end{aligned} \tag{11}$$

Next, by substituting (11) into (8), the cost function can be expressed as,

$$\begin{aligned} &\min_{K} \sum_{i=1}^{r} \lambda_{\max}\left((\hat{E}_x^i)^{-1} P_i (\hat{E}_x^i)^{-T}\right) \\ &\text{s.t.} \quad P(A+BK) + (A+BK)^T P + C^T C = 0. \end{aligned} \tag{12}$$

Now, by introducing variables $s_i \in \mathbb{R}, \mathrm{s}_i > 0$, for every $i \in \mathbb{Z}_{[1,r]}$, the following upper-bound holds:

$$\lambda_{\max}((\hat{E}_x^i)^{-1} P_i (\hat{E}_x^i)^{-T}) \le \frac{1}{s_i}. \quad (13)$$

Equation (13) is equivalent to the SDP constraint as below

$$Q_i - s_i (E_x^i)^{-1} \ge 0, \quad (14)$$

where $Q_i \ge 0, Q_i = P_i^{-1}$, for every $\forall i \in \mathbb{Z}_{[1,r]}$, and where we defined $Q = \text{blkdiag}(Q_i)$. Using the Schur complement and defining the new decision variable $Y = KQ$, (12) can be equivalently formulated as:

$$\min_{s_i, Q_i \ge 0, Y} \sum_{i=1}^{r} \frac{1}{s_i}$$

$$\text{s.t.} \quad Q_i - s_i (E_x^i)^{-1} \ge 0, \forall i \in \mathbb{Z}_{[1,r]}, \quad (15)$$

$$\begin{bmatrix} (AQ+BY)+(AQ+BY)^T & QC^T \\ CQ & -I \end{bmatrix} \ge 0.$$

We will now focus on the input constraints (9).

c) Robustness to Perturbations on the Initial States: According to (7) and (9), it is required that $u_j(t)^T E_u^j u_j(t) \le 1$ for every $j \in \mathbb{Z}_{[1,q]}$, and every time instant $t \in \mathbb{R}_0^+$, where $u_j(t) = K_j x(t)$, and $K = \text{blkcol}(K_j)$. This is equivalent to requiring that $x(t)^T K_j^T E_u^j K_j x(t) \le 1$ for every $j \in \mathbb{Z}_{[1,q]}$, and every time instant $t \in \mathbb{R}_0^+$. Recall that the Lyapunov matrix P defines level sets for the controlled state trajectories, in the sense that $x(t_1)^T P x(t_1) \le k$ for some $k > 0$ and $t_1 \in \mathbb{R}_0^+$ implies that $x(t)^T P x(t) \le k$ for every $t > t_1$. Also, notice that

$$x(0)^T P x(0) \le \max_{x_0 \in \chi_0} x(0)^T P x(0) \le \sum_{i=1}^{r} \frac{1}{s_i}, \quad (16)$$

which is equivalent to $x(0)^T \frac{P}{\sum_{i=1}^{r} \frac{1}{s_i}} x(0) \le 1$. We conclude that the constraints on the input signals can be formulated as

$$K_j^T E_u^j K_j \le \frac{P}{\sum_{i=1}^{r} \frac{1}{s_i}}, \quad \forall j \in \mathbb{Z}_{[1,q]}, \quad (17)$$

which is equivalent to $Q - Y_j^T E_u^j \sum_{i=1}^{r} \frac{1}{s_i} Y_j \ge 0$. By exploiting the Schur complement the former can be written as

$$\begin{bmatrix} Q & Y_j^T \\ Y_j & (E_u^j)^{-1} (\sum_{i=1}^{r} \frac{1}{s_i})^{-1} \end{bmatrix} \ge 0, \quad \forall j \in \mathbb{Z}_{[1,q]}. \quad (18)$$

Notice that if $r = 1$, then (18) is a SDP constraint and the problem (15), (18) admits an equivalent convex formulation by maximizing s instead of minimizing $\frac{1}{s}$. Further elaboration is needed if $r > 1$. Indeed, in our case $r = 15$.

d) Convex Formulation of (18): The harmonic mean of the decision variable $s_i, i \in \mathbb{Z}_{[1,r]}$, is defined as

$$h(s) = \frac{r}{\sum_{i=1}^{r} \frac{1}{s_i}}. \quad (19)$$

Our approach is based on lower bounding the harmonic mean by introducing an additional decision variable w, subject to $w \le h(s)$. First, notice that $w \le h(s)$ is equivalent to

$$\sum_{i=1}^{r} \frac{w^2}{s_i} \le rw, \quad (20)$$

Next, we introduce a set of decision variables $y_i, \forall i \in \mathbb{Z}_{[1,r]}$, which allows us to cast (20) as

$$w^2 \le s_i y_i, \forall i \in \mathbb{Z}_{[1,r]}, \quad (21)$$

$$\sum_{i=1}^{r} y_i = rw. \quad (22)$$

Equation (21) describes a rotated cone and can thus be expressed as the following Second Order Cone Programming constraint:

$$\left\| \begin{matrix} 2w \\ s_i - y_i \end{matrix} \right\|_2 \le s_i + y_i, \quad \forall i \in \mathbb{Z}_{[1,r]}. \quad (23)$$

We conclude that the problem (8)-(10) admits the following tractable SDP formulation:

$$\max_{s_i, Q_i \ge 0, Y, w, y_i} w$$

$$\text{s.t.} \quad Q_i - s_i (E_x^i)^{-1} \ge 0, \quad \forall i \in \mathbb{Z}_{[1,r]},$$

$$\begin{bmatrix} (AQ+BY)+(AQ+BY)^T & QC^T \\ CQ & -I \end{bmatrix} \ge 0,$$

$$\begin{bmatrix} Q & Y_j^T \\ Y_j & (E_u^j)^{-1} \frac{w}{r} \end{bmatrix} \ge 0, \quad \forall j \in \mathbb{Z}_{[1,q]}, \quad (24)$$

$$\left\| \begin{matrix} 2w \\ s_i - y_i \end{matrix} \right\|_2 \le s_i + y_i, \quad \forall i \in \mathbb{Z}_{[1,r]},$$

$$\sum_{i=1}^{r} y_i = rw, \quad Q = \text{blkdiag}(Q_i), \quad Y = \text{blkcol}(Y_j),$$

Y is decentralized.

Notice that, thanks to the fact that Q is block-diagonal, those entries of Y that are required to be null are also null in matrix K.

D. Simulation Results

An analysis has been performed to study the effect of the wind variability on the operating point of the HVDC grid, and the corresponding impact on the optimization procedure. Each wind scenario, results in a different operating condition, which is the point around which the nonlinear equations of (2)-(3) are linearized. Hence, the *A*, *B* matrices in (2)-(3) are dependent on the wind scenario. The DC voltage stability index, *J*, is calculated for various operating

Table II: DC voltage stability indices of the 4-terminal HVDC test grid under different scenarios (different added HVDC links and different AC current *d*-component references).

Added HVDC link	Added HVDC link's Length (km)	AC current d-component reference in per unit	DC voltage stability index	AC current d-component reference in per unit	DC voltage stability index	AC current d-component reference in per unit	DC voltage stability index	AC current d-component reference in per unit	DC voltage stability index	$i_{d,ref,1}$: Johan-Sverdrup reference
1-3	600	$i_{d,ref,1}$ -0.125	**3.73**	$i_{d,ref,1}$ -0.125	**4.10**	$i_{d,ref,1}$ -0.125	**3.98**	$i_{d,ref,1}$ -0.125	**3.71**	-0.125
1-4	750	$i_{d,ref,2}$ 0.75	**4.21**	$i_{d,ref,2}$ 0.75	**4.16**	$i_{d,ref,2}$ 0.75	**3.63**	$i_{d,ref,2}$ 0.75	**2.93**	
2-3	650	$i_{d,ref,3}$ -0.125	**5.08**	$i_{d,ref,3}$ -0.375	**4.84**	$i_{d,ref,3}$ -0.625	**5.09**	$i_{d,ref,3}$ -0.875	**3.50**	
2-4	800	$i_{d,ref,4}$ -0.5	**5.59**	$i_{d,ref,4}$ -0.25	**5.09**	$i_{d,ref,4}$ 0	**5.25**	$i_{d,ref,4}$ 0.25	**3.89**	
1-3	600	$i_{d,ref,1}$ -0.375	**3.87**	$i_{d,ref,1}$ -0.375	**4.19**	$i_{d,ref,1}$ -0.375	**3.89**	$i_{d,ref,1}$ -0.375	**3.80**	-0.375
1-4	750	$i_{d,ref,2}$ 0.75	**5.23**	$i_{d,ref,2}$ 0.75	**3.80**	$i_{d,ref,2}$ 0.75	**3.30**	$i_{d,ref,2}$ 0.75	**3.95**	
2-3	650	$i_{d,ref,3}$ -0.125	**4.83**	$i_{d,ref,3}$ -0.375	**5.04**	$i_{d,ref,3}$ -0.625	**3.64**	$i_{d,ref,3}$ -0.875	**3.78**	
2-4	800	$i_{d,ref,4}$ -0.25	**5.34**	$i_{d,ref,4}$ 0	**5.28**	$i_{d,ref,4}$ 0.25	**3.79**	$i_{d,ref,4}$ 0.5	**3.91**	
1-3	600	$i_{d,ref,1}$ -0.625	**4.01**	$i_{d,ref,1}$ -0.625	**4.10**	$i_{d,ref,1}$ -0.625	**3.85**	$i_{d,ref,1}$ -0.625	**3.92**	-0.625
1-4	750	$i_{d,ref,2}$ 0.75	**3.86**	$i_{d,ref,2}$ 0.75	**3.70**	$i_{d,ref,2}$ 0.75	**3.80**	$i_{d,ref,2}$ 0.75	**3.52**	
2-3	650	$i_{d,ref,3}$ -0.125	**5.00**	$i_{d,ref,3}$ -0.375	**3.63**	$i_{d,ref,3}$ -0.625	**3.76**	$i_{d,ref,3}$ -0.875	**3.49**	
2-4	800	$i_{d,ref,4}$ 0	**5.33**	$i_{d,ref,4}$ 0.25	**3.80**	$i_{d,ref,4}$ 0.5	**3.87**	$i_{d,ref,4}$ 0.75	**4.00**	
1-3	600	$i_{d,ref,1}$ -0.875	**3.57**	$i_{d,ref,1}$ -0.875	**3.85**	$i_{d,ref,1}$ -0.875	**3.92**	$i_{d,ref,1}$ -0.875	**3.82**	-0.875
1-4	750	$i_{d,ref,2}$ 0.75	**3.29**	$i_{d,ref,2}$ 0.75	**3.51**	$i_{d,ref,2}$ 0.75	**3.84**	$i_{d,ref,2}$ 0.75	**4.25**	
2-3	650	$i_{d,ref,3}$ -0.125	**3.52**	$i_{d,ref,3}$ -0.375	**3.69**	$i_{d,ref,3}$ -0.625	**3.59**	$i_{d,ref,3}$ -0.875	**3.69**	
2-4	800	$i_{d,ref,4}$ 0.25	**3.93**	$i_{d,ref,4}$ 0.5	**3.94**	$i_{d,ref,4}$ 0.75	**4.01**	$i_{d,ref,4}$ 1	**3.99**	
$i_{d,ref,3}$: BorWin1 reference		-0.125		-0.375		-0.625		-0.875		

points that are correlated with different wind speeds and corresponding wind power extractions

Implementing (24) is simple by using the YALMIP toolbox [20] of Matlab® in combination with the MOSEK [21] solver. Once the optimal solution $(Q^*, Y^*, s^*, w^*, y^*)$ is obtained, it is possible to retrieve the worst initial perturbation $x(0)^{worst}$, the worst-case performance parameter J^*, and the corresponding optimal controller K^* as follows. Compute $P^* = (Q^*)^{-1}$. For each $j \in \mathbb{Z}_{[1,q]}$, compute $x(0)_i^{worst}$ as the eigenvector associated with the maximum eigenvalue of matrix $(\hat{E}_x^i)^{-1} P_i^* (\hat{E}_x^i)^{-T}$. Then $x(0)^{worst} = \mathrm{col}(x(0)_i^{worst})$, $J^* = x(0)^{worst^T} P^* x(0)^{worst}$ and $Y^* = K^* Q^*$. Naturally, the performance J^* can also be computed via simulation, by setting the initial state $x(0)^{worst}$, applying the controller K^* and integrating the trajectory of $z(t) = Cx(t)$ over time until steady state is achieved.

Although we kept the derivation general, we remind the reader that the model (2), (3) will be used for the purpose of this paper. For the considered model we thus have that, $n = p = 23$, $m = 8$, $j = 4$, and $m_j = 2$, for every j and n_i is equal to 1 or 2 depending on the different scalar state variables, which are coupled or uncoupled, as per (4).

The matrices $E_u^j, \forall j \in \mathbb{Z}_{[1,q]}$, are chosen as diagonal matrices enforcing (9) with the *dq*-reference currents at each terminal to be bounded as follows:

$$|\Delta i_{ref,n}| = \sqrt{\Delta i_{d,ref,n}^2 + \Delta i_{q,ref,n}^2} \le 0.5 \ p.u.. \quad (25)$$

Similarly, the matrices $E_x^i, \forall i \in \mathbb{Z}_{[1,r]}$, are also diagonal matrices to impose constraints (9) on the maximum allowed deviations of the initial state variables (26-29). The AC current boundaries are extracted from [22], and the DC current and voltage limitations correspond to the physical characteristics of the DC cable.

$$|\Delta i_n| = \sqrt{\Delta i_{d,n}^2 + \Delta i_{q,n}^2} \le 0.1 \ p.u., \quad (26)$$

$$|\Delta v_{dc,n}| \le 0.1 \ p.u., \quad (27)$$

$$|\Delta g_n| = \sqrt{\Delta g_{d,n}^2 + \Delta g_{q,n}^2} \le 0.01 \ p.u., \quad (28)$$

$$|\Delta i_{dc,n}| \le 0.1 \ p.u.. \quad (29)$$

Simulation results for different scenarios are presented in Table II. Wind farm operating points are selected to be the average of each normalized power range considered in Table I. These four values are applied to the offshore converters 1 and 3 forming 16 different scenarios, which change the trajectory along which we linearize. Converter 2 operating condition is kept constant at 0.75 per unit, corresponding to a passive load, constantly absorbing a fixed amount of power. Converter 4 is representative of the slack bus and ensures the grid power balance. As can be seen in Table II, the DC voltage stability index value, which is representative of the DC voltage oscillation under worst-case initial condition, varies from one scenario to another. The reference current, $i_{d,ref,1}$, is representative of the *d*-component of the AC current reference at Johan-Sverdrup whereas $i_{d,ref,3}$, is the *d*-component of the AC current reference at BorWin 1. Since the AC voltage *d*-component references at the four terminals are assumed to be one per unit (base voltage: 400 kV), the per unit average power values can be substituted by the per unit current values. Performance indices are calculated for the 16 possible scenarios considering four different grid topologies, which are based on the connection of the two point-to-point HVDC networks through the four different HVDC links. The optimal DC voltage stability index (the minimum value) at every scenario is highlighted in green. In eight different scenarios, the addition of the HVDC link 1-4 results in the optimal DC voltage stability index while addition of the HVDC links 1-3 and 2-3, lead to the optimal solution in two and six cases, respectively. Addition of the

Table III: DC voltage stability index at nominal condition versus average DC voltage stability index.

Added HVDC link	Added HVDC link's Length (km)	DC voltage stability index at nominal condition	Average DC voltage stability index
1-3	600	3.82	3.88
1-4	750	4.25	3.96
2-3	650	3.69	4.37
2-4	800	3.99	4.71

HVDC link 2-4 does not lead to minimum DC voltage oscillation in any of the scenarios.

The radial network, which is the result of the connection of the two point-to-point HVDC grids through the link 2-3 provides the optimal DC voltage stability index when $i_{d,ref,1}$ and $i_{d,ref,3}$ are both generating - 0.875 per unit power. This scenario is assumed to represent the nominal operating condition of the system, being the closest to the nominal power capacity of both wind farms. This would be the only scenario taken into consideration if only nameplate information (and no wind time-series) was available for the wind farms. To further consider the probability of the occurrence of each operating condition, the average DC voltage stability criterion was estimated. The average DC voltage stability index is calculated as the sum of all the products between the DC voltage stability indices and the corresponding event probability given in Table I. Therefore, the optimal HVDC link expansion option ensuring the best stability performance at worst-case initial condition is the link with the lowest average DC voltage stability index. As can be seen in Table III, the HVDC link between the substations 1 and 3 gives the lowest average DC voltage stability index and, hence, the optimal solution from the stabilization standpoint. On the other hand, link 2-3 provides the optimal solution under the nominal operating condition. Therefore, if the assessment of the stability index was only based on the nominal operating condition (i.e. the assumption of full power production of the wind farms) and the intermittency of wind speed was not taken into account, it could have misguided to the selection of the link 2-3 as the new HVDC link.

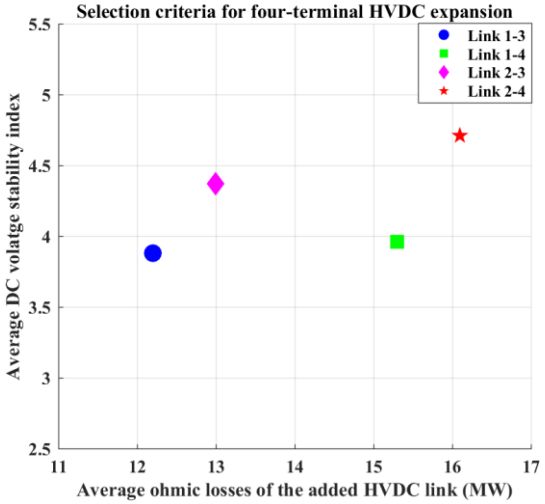

Fig. 4: Comparison of the considered expansion options.

Finally, we assess the expansion problem based on the two (equally weighted) criteria of: a) minimum average ohmic cable losses; and b) minimum average DC voltage stability index (i.e. minimum DC voltage oscillations). Average ohmic cable losses are calculated for every added HVDC link with the same procedure as the average DC voltage stability index by taking the probability of occurrence of every operating scenario into account. In the presented case, link 1-3 is the best option according to both criteria and it represents the point at minimum distance from the origin according to Fig. 4. Therefore, it should be the final choice in the expansion decision. However, if different weights are allocated to the different criteria based on specific expansion planning priorities, different preferable configurations may be selected.

III. Conclusions

This paper presents an approach to minimize DC voltage oscillations in a multi-terminal HVDC grid, taking into account how the wind variability affects the power production of connected wind farms. The selected test case considers the placement of a new HVDC link between two separate point-to-point HVDC grids. The goal is to identify the link that ensures minimum DC voltage variations under worst-case initial perturbation, and the decentralized linear controller that guarantees such performance. The expansion choice is made considering that different links contribute differently to the grid stabilization, depending on the specific operating conditions induced by the wind variability. It is shown that taking the latter effect into account leads to a different expansion decision than working under the simplifying assumption that wind farms always provide a nominal power production. Finally, active power loss on the DC cables is considered as an additional criterion to orient the expansion decision, and it is shown that in the specific case both criteria identify link 1-3 as the best expansion alternative.

Acknowledgment

Authors A. Elahidoost and E. Tedeschi are working under the project of "Integrated Design and Control of Offshore HVDC Networks (IDeCON)" financially supported by the Norwegian Research Council and DNV GL. The work of M. Kamgarpour and L. Furieri is gratefully supported by the ERC Starting Grant CONENE.

References

[1] "Wind in power 2017: Annual combined onshore and offshore wind energy statistics," WindEurope, February 2018, Available: https://windeurope.org/wp-content/uploads/files/about wind/statistics/WindEurope-Annual-Statistics-2017.pdf

[2] "Wind energy in Europe: Scenarios for 2030," WindEurope, September 2017, Available: https://windeurope.org/wp-content/uploads/files/about-wind/reports/Wind-energy-in-Europe-Scenarios-for-2030.pdf.

[3] D. Connolly, H. Lund, and B. V. Mathiesen, "Smart energy Europe: The technical and economic impact of one potential 100% renewable energy scenario for the European Union," *Renewable and Sustainable Energy Reviews*, vol. 60, pp. 1634-1653, 2016/07/01/ 2016.

[4] W. Wang and M. Barnes, "Power flow algorithms for multi-terminal VSC-HVDC with droop control," *IEEE Transactions on Power Systems*, vol. 29, no. 4, pp. 1721-1730, 2014.

[5] G. Pinares and M. Bongiorno, "Analysis and mitigation of instabilities originated from DC-side resonances in VSC-HVDC systems," *IEEE Transactions on Industry Applications*, vol. 52, no. 4, pp. 2807-2815, 2016.

[6] A. H. Dominguez, A. H. Escobar, and R. A. Gallego, "An MILP model for the static transmission expansion planning problem including HVAC/HVDC links, security constraints and power losses with a reduced search space," *Electric Power Systems Research*, vol. 143, pp. 611-623, 2// 2017.

[7] A. H. Dominguez, L. H. Macedo, A. H. Escobar, and R. Romero, "Multistage security-constrained HVAC/HVDC transmission expansion planning with a reduced search space," *IEEE Transactions on Power Systems*, vol. PP, no. 99, pp. 1-1, 2017.

[8] H. Ergun, B. Rawn, R. Belmans, and D. V. Hertem, "Stepwise investment plan optimization for large scale and multi-zonal transmission system expansion," *IEEE Transactions on Power Systems*, vol. 31, no. 4, pp. 2726-2739, 2016.

[9] S. S. Torbaghan, M. Gibescu, B. G. Rawn, and M. v. d. Meijden, "A market-based transmission planning for HVDC grid - Case study of the North Sea," *IEEE Transactions on Power Systems*, vol. 30, no. 2, pp. 784-794, 2015.

[10] M. K. Bucher, R. Wiget, G. Andersson, and C. M. Franck, "Multiterminal HVDC networks - What is the preferred topology?," *IEEE Transactions on Power Delivery*, vol. 29, no. 1, pp. 406-413, 2014.

[11] A. Elahidoost and E. Tedeschi, "Expansion of offshore HVDC grids: An overview of contributions, status, challenges and perspectives," in *2017 IEEE 58th International Scientific Conference on Power and Electrical Engineering of Riga Technical University (RTUCON)*, 2017, pp. 1-7.

[12] J. L. Rueda, W. H. Guaman, J. C. Cepeda, I. Erlich, and A. Vargas, "Hybrid approach for power system operational planning with smart grid and small-signal stability enhancement considerations," *IEEE Transactions on Smart Grid*, vol. 4, no. 1, pp. 530-539, 2013.

[13] A. Nikoobakht, J. Aghaei, T. Niknam, V. Vahidinasab, H. Farahmand, and M. Korpås, "Towards robust OPF solution strategy for the future AC/DC grids: Case of VSC-HVDC-connected offshore wind farms," *IET Renewable Power Generation*, vol. 12, no. 6, pp. 691-701, 2018.

[14] H. Svendsen, "Hourly wind and solar energy time series from reanalysis dataset," 2017, Available: http://hdl.handle.net/11250/2468143.

[15] I. Graabak, H. Svendsen, and M. Korpås, "Developing a wind and solar power data model for Europe with high spatial-temporal resolution," in *2016 51st International Universities Power Engineering Conference (UPEC)*, 2016, pp. 1-6.

[16] W. Leterme, N. Ahmed, J. Beerten, L. Angquist, D. V. Hertem, and S. Norrga, "A new HVDC grid test system for HVDC grid dynamics and protection studies in EMT-type software," in *AC and DC Power Transmission, 11th IET International Conference on*, 2015, pp. 1-7.

[17] A. Elahidoost, L. Furieri, E. Tedeschi, M. Kamgarpour "Optimizing HVDC grid expansion and control for enhancing DC stability," *IEEE PSCC 2018*, Dublin, Ireland, 2018, in press.

[18] A. Fuchs and M. Morari, "Actuator performance evaluation using LMIs for optimal HVDC placement," in *2013 European Control Conference (ECC)*, 2013, pp. 1529-1534.

[19] A. Fuchs and M. Morari, "Placement of HVDC links for power grid stabilization during transients," in *2013 IEEE Grenoble Conference*, 2013, pp. 1-6.

[20] J. Löfberg, "Yalmip: A toolbox for modeling and optimization in MATLAB," in *Proceeding of the CACSD*, Taipei, Taiwan, 2004.

[21] E.D. Anderson, K.D. Andersen, "The Mosek interior point optimizer for linear programming: An implementation of the homogeneous algorithm," In: H. Frenk, T. Terlaky, S. Zhang (eds), *High Performance Optimization*, Applied Optimization, vol. 33, Springer, Boston, MA, 2000.

[22] R. Wachal, et al., "Guide for the development of models for HVDC converters in a HVDC grid," CIGRE, Working Group B4.57, December 2014.